Solid State Ionics 288 (2016) 120–123

Contents lists available at ScienceDirect

Solid State Ionics

journal homepage: www.elsevier.com/locate/ssi

Nickel nanocatalyst exsolution from (La,Sr) (Cr,M,Ni)O_3 (M=Mn,Fe) perovskites for the fuel oxidation layer of Oxygen Transport Membranes

D. Papargyriou, J.T.S. Irvine

School of Chemistry, University of St Andrews, North Haugh, St Andrews, Fife KY16 9ST, UK

ARTICLE INFO

Article history:
Received 28 July 2015
Received in revised form 13 October 2015
Accepted 5 November 2015
Available online 28 November 2015

Keywords:
Perovskites
Exsolution
Catalyst
Fuel oxidation layer

ABSTRACT

$La_{0.75}Sr_{0.25}Cr_{0.5}Mn_{0.5}O_3$ (LSCM) and $La_{0.75}Sr_{0.25}Cr_{0.5}Fe_{0.5}O_3$ (LSCF) perovskites with partial substitution of the B-site by 5 mol% of Ni were synthesised and characterised for the fuel oxidation layer of Oxygen Transport Membranes (OTMs). X-ray diffraction showed that single phase compounds were obtained at 1300 °C. LSCM exhibits a rhombohedral structure and LSCF an orthorhombic structure. Both materials retain their structures, after doping the B site with Ni, with small changes on the unit cell parameters. Thermal analysis under reducing conditions was used to investigate the reducibility of these perovskites up to 900 °C, which appears to be enhanced by doping with Ni. The formation of Ni nanoparticles (30–50 nm) on the LSCMNi and LSCFNi grains was observed by scanning electron microscopy, after reducing the samples in 5% H_2/Ar at 900 °C, indicating possible enhanced catalytic activity and potential benefits for the development of the OTMs. DC conductivity measurements conducted under a redox cycle, indicate that LSCFNi presents a better redox stability than LSCMNi.

1. Introduction

Oxygen Transport Membranes (OTMs) offer a promising technology for directly supplying oxygen to a fuel gas for the purpose of generating syngas or heat [1]. In this project, the OTM is based upon an inactive support that sequentially has a fuel oxidation layer, a dense layer and a reduction layer, which are a combination of perovskites and fluorites. In order to improve the fuel oxidation layer's performance, the incorporation of a catalyst in the perovskite lattice is necessary. As the fuel oxidation layer is deeply buried in the structure the traditional method of direct impregnation of a solution containing desired cations would be difficult, not to mention wasteful, costly and time consuming. The in situ nanocatalyst exsolution appears to be the best approach to solve this problem. Redox exsolution tends to grow pinned metal nanoparticles on the reduced oxide surface [2] offering excellent possible catalytic properties and the possibility to regenerate the nanostructure via a redox cycle [3].

$La_{0.75}Sr_{0.25}Cr_{0.5}Mn_{0.5}O_3$ appears to be a good candidate material, as it has been reported as a good catalyst for the full oxidation of CH_4 [4] and it can exsolve Ni [5,6] or Ru [7] nanoparticles on the surface.

Another material that has been reported as a good catalyst for the partial oxidation of CH_4 and reforming at temperatures above 850 °C is $La_{0.75}Sr_{0.25}Cr_{0.5}Fe_{0.5}O_3$ [8] and the Ni exsolution will be investigated for this material.

2. Experimental section

2.1. Synthesis

Powders of $La_{0.75}Sr_{0.25}Cr_{0.5}Mn_{0.5}O_3$ (LSCM), $La_{0.75}Sr_{0.25}Cr_{0.475}Mn_{0.475}Ni_{0.05}O_3$ (LSCMNi), $La_{0.75}Sr_{0.25}Cr_{0.5}Fe_{0.5}O_3$ (LSCF) and $La_{0.75}Sr_{0.25}Cr_{0.475}Fe_{0.475}Ni_{0.05}O_3$ (LSCFNi) were synthesized by a modified sol–gel synthesis [7]. The starting metallic salts used were lanthanum nitrate hexahydrate (99.99%) (Alfa Aesar), strontium nitrate (>99%) (Sigma Aldrich), chromium nitrate nonahydrate (99%) (Sigma Aldrich), manganese acetate tetrahydrate (>99%) (Alfa Aesar), iron nitrate nonahydrate (Sigma Aldrich) and nickel nitrate hexahydrate (Acros Organics). The proper stoichiometric ratio of citric acid and ethylene glycol was diluted in distilled water under magnetic stirring. When the solution became clear, all the precursors were added slowly and the temperature was increased at ~80 °C. After one hour under stirring and when complete dissolution of the salts was achieved, the temperature was increased at 100–120 °C and the solution was kept under heating and stirring until it evaporated, resulting a gel. Finally, the temperature was gradually increased at 300 °C, until the gel was combusted to a black powder. The obtained powders were treated in air at 1300 °C for 4 h, in order to get a pure phase material.

The reduction of the powder samples was carried out in a tube furnace, at 900 °C for 20 h, in a controlled-atmosphere furnace supplied with 5% H_2/Ar, in order to exsolve the catalyst nanoparticles on the surface of the perovskite.

http://dx.doi.org/10.1016/j.ssi.2015.11.007

2.2. Characterisation techniques

Room temperature powder X-ray diffraction (XRD) was performed on a PANalytical Empyrean diffractometer. The obtained XRD patterns were analysed with STOE Win XPOW software in order to determine phase purity, the crystal structure and the cell parameters of the samples. Thermogravimetric analysis (TGA) was performed using a Netzsch STA 449C instrument equipped with Proteus thermal analysis software. The TGA studies were carried out under reducing conditions (5% H_2/Ar) from room temperature to 900 °C, in order to determine the weight change of the perovskite during the reduction. The microstructure of the samples' surface was analysed using a JEOL JSM-6700 field emission 74 scanning electron microscope (FEG-SEM). The total conductivity of the samples was measured using a conventional four-terminal method. Bar samples were prepared by calcination at 1300 °C for 1 h. Gold wire contacts were attached to the bars, which then were cured at 850 °C for 1 h. The conductivity of the samples was measured under a redox cycle at 900 °C. Low oxygen partial pressure was achieved by using a continuous flow of 5% H_2/Ar.

3. Results–discussion

3.1. Structure

The structure of the different samples was analysed by XRD after calcination at 1300 °C for 4 h. Fig. 1 shows the XRD patterns of LSCM and LSCMNi. LSCM presents a rhombohedral structure and after doping the B-site with 5 mol% Ni it retains this structure with a small decrease of the unit cell parameters, as presented in table 1. This decrease of the cell parameters after doping LSCM with Ni has been also reported by Jardiel et al. [5] More specifically, it was observed that the more Ni is added on the B-site of LSCM the more the cell volume is decreasing. This behaviour was explained by the fact that when Ni is doped on the B-site, Mn^{3+}, with an ionic radius 0.65 Å, tends to change to Mn^{4+}, with an ionic radius 0.53 Å, leading to a decrease of the unit cell parameters. Fig. 2 presents the XRD patterns of LSCF and LSCFNi. LSCF shows an orthorhombic structure and after doping the B-site with 5 mol% Ni it retains this structure with a small decrease of the cell parameters (Table 1), presenting a similar behaviour with the LSCM based materials.

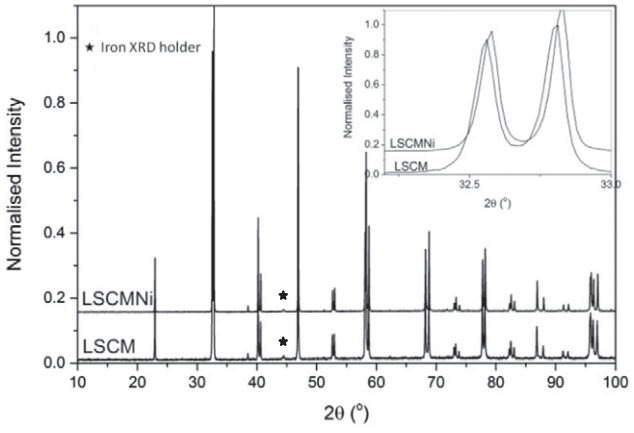

Fig. 1. XRD pattern of LSCM and LSCMNi.

Table 1
Unit cell parameters for LSCM, LSCMNi, LSCF and LSCFNi.

	LSCM	LSCMNi	LSCF	LSCFNi
Space Group	$R\bar{3}c$	$R\bar{3}c$	Pnma	Pnma
a (Å)	5.4962 (10)	5.49242 (14)	5.4925 (4)	5.4868 (13)
b (Å)	–	–	5.5326 (3)	5.5299 (6)
c (Å)	13.3196 (14)	13.3036 (4)	7.7645 (6)	7.7628 (14)
Volume (Å^3)	348.46 (8)	347.557 (13)	235.947 (20)	235.54 (5)

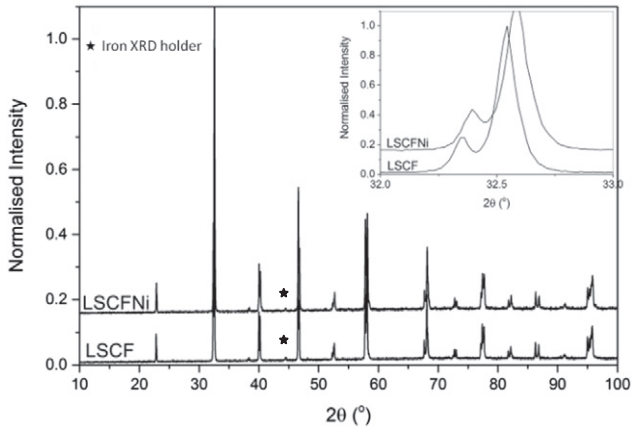

Fig. 2. XRD pattern of LSCF and LSCFNi.

3.2. Thermal analysis

The weight change under reducing conditions (5% H_2/Ar) was investigated for the Ni doped and undoped samples up to 900 °C. As presented in Figs. 3 and 4, the weight for all the samples is decreasing and this loss is taking place in one step, which corresponds to the oxygen loss from the perovskite lattice due to the reduction. When doping LSCM

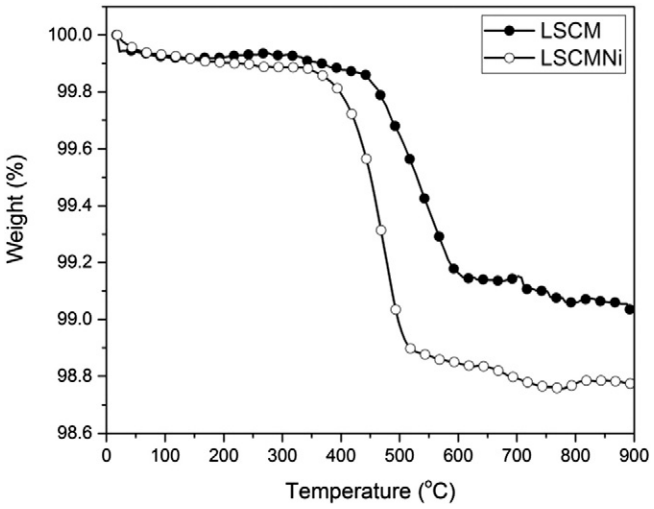

Fig. 3. TGA of LSCM and LSCMNi under 5% H_2/Ar.

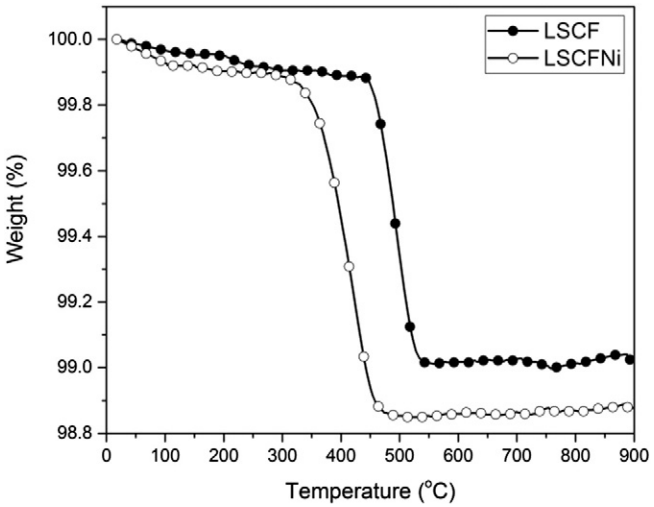

Fig. 4. TGA of LSCF and LSCFNi under 5% H_2/Ar.

and LSCF with Ni, it appears that, even if the samples present the same trend, the reduction is happening at slightly lower temperatures for the Ni doped samples and is leading to a larger weight loss. That indicates that the presence of Ni in the perovskite lattice is increasing its reducibility, which is consistent with prior reports [5].

More specifically, for the LSCM-based materials the main extent of the reduction is taking place between 400 and 600 °C and corresponds to a weight loss of 0.95% for LSCM and 1.23% for LSCMNi, which is 0.135 and 0.175 oxygen per formula unit, respectively. Comparable behaviour has been reported for LSCM under reducing conditions (10% H_2/90% Ar) up to 970 °C by Jen-Hau Wan et al. [9]

Fig. 4 shows the weight change of LSCF with and without Ni doping under reducing conditions. The main weight loss is occurring between 300 and 550 °C for the LSCF-based materials and corresponds to a weight loss of 0.97% for LSCF and 1.11% for LSCFNi, which is 0.139 and 0.159 oxygen per formula unit, respectively.

3.3. Nickel exsolution

The LSCMNi and LSCFNi samples were reduced at 900 °C for 20 h, under 5% H_2/Ar in order to exsolve the Ni catalyst on the perovskite surface. The SEM images in Figs. 5 and 6 present the exsolution of Ni nanoparticles, with diameter between 30 and 50 nm, on the surface of LSCMNi and LSCFNi. This behaviour is consistent with previous reports by Jardiel et al. [5]

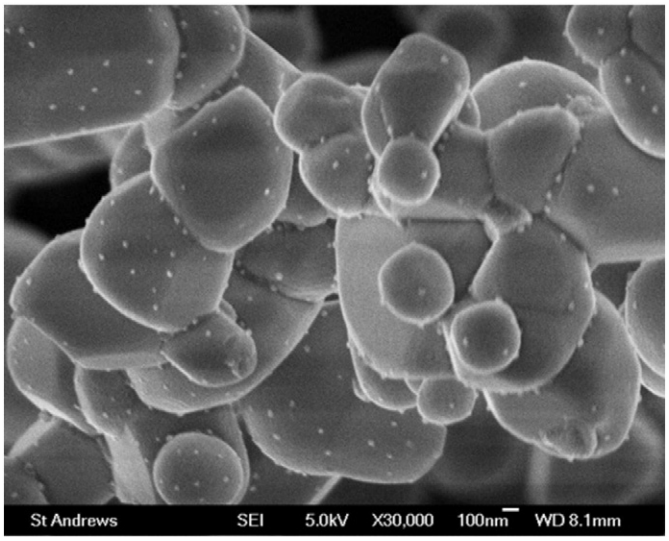

Fig. 5. SEM micrograph of LSCMNi after reduction at 900 °C for 20 h.

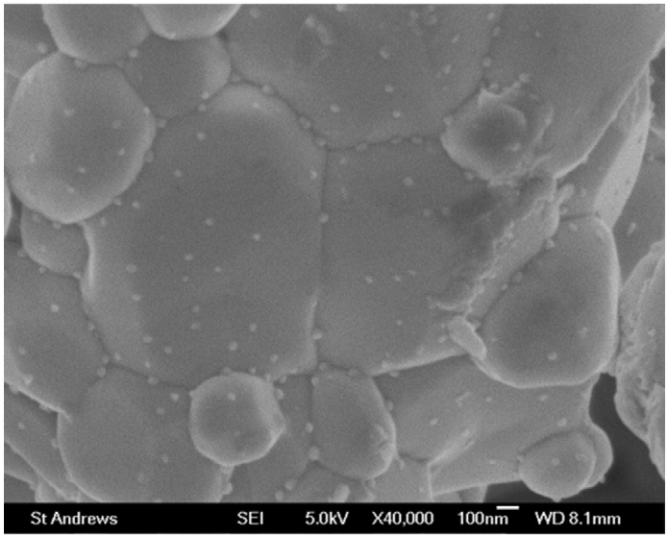

Fig. 6. SEM micrograph of LSCFNi after reduction at 900 °C for 20 h.

3.4. DC conductivity

The total conductivity of LSCM, LSCMNi, LSCF and LSCFNi porous bar samples was measured during a redox cycle at 900 °C. The samples were heated up to 900 °C in air and when the conductivity values were stabilised, 5% H_2/Ar was introduced and the perovskites were reduced overnight. After that, the samples were re-oxidised by introducing air until the conductivity value reached a plateau.

Fig. 7 presents how the conductivity changes under reducing conditions at 900 °C. When 5% H_2/Ar is introduced the conductivity values drop fast by around two orders of magnitude. The decrease of the conductivity value on reduction is consistent with p-type conduction and is occurring due to the oxygen loss from the perovskite lattice [10]. However, the conductivity value for LSCM is decreasing less than the other materials. This could be an indication that the presence of Fe or Ni enhances the p-type conductivity.

Fig. 8 presents the re-oxidation of the samples and how the conductivity changes at 900 °C. This procedure appears to be slower than

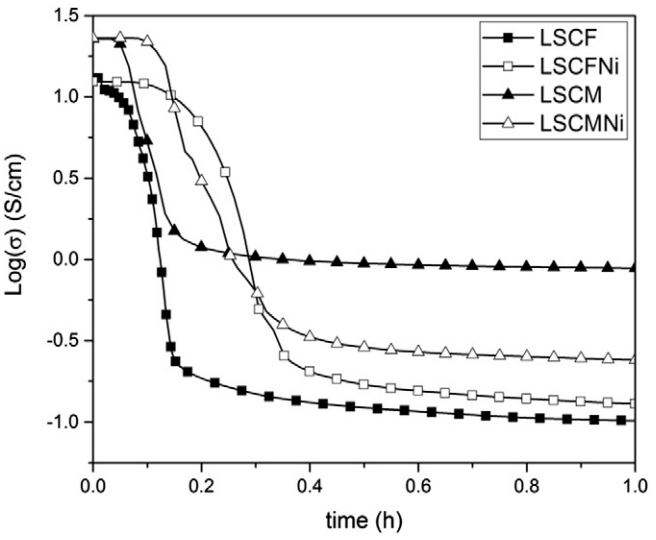

Fig. 7. DC conductivity of LSCM(Ni) and LSCF(Ni) at 900 °C during reduction (5% H_2/Ar).

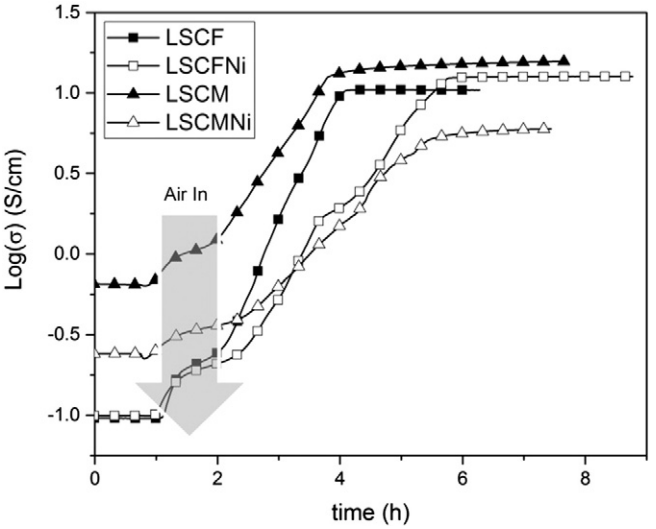

Fig. 8. DC conductivity of LSCM(Ni) and LSCF(Ni) at 900 °C during re-oxidation (air).

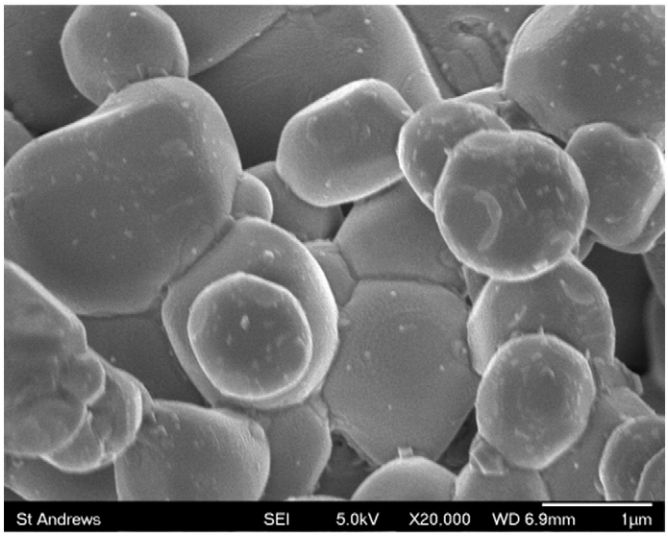

Fig. 9. SEM micrograph of LSCMNi reduced at 900 °C for 20 h after the redox cycle.

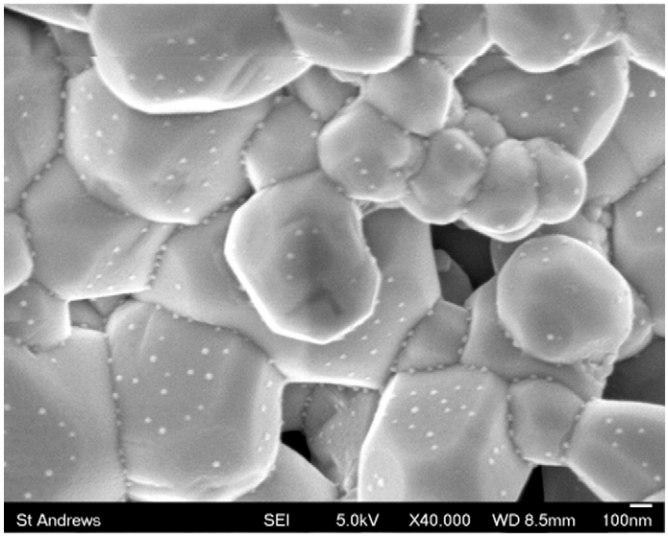

Fig. 10. SEM micrograph of LSCFNi reduced at 900 °C for 20 h after the redox cycle.

reduction and after a few hours the conductivity values increase close to the initial values. However, LSCMNi does not reach the initial conductivity value after the redox cycle, indicating possible degradation of the material.

After the redox cycle, the Ni doped samples were re-reduced at 900 °C for 20 h in order to investigate how the formation of the nanoparticles is affected by this treatment. Fig. 9 shows that LSCMNi exsolves different shape particles and most of them appear to be merged. This could also explain the drop in the conductivity value after the redox cycle and could be an indication of sample degradation. LSCFNi appears to exsolve Ni nanoparticles nicely on the perovskite surface after this treatment (Fig. 10), indicating better redox stability.

4. Conclusions

LSCMNi and LSCFNi were synthesised and characterised for the fuel oxidation layer of the OTMs. Ni nanoparticles of 30–50 nm were exsolved on the surface of these perovskites, indicating possible improvement of the catalytic properties of these materials and benefits for the development of the OTMs. The redox cycle performed, indicates that LSCFNi presents better redox stability than LSCMNi and possibly will be a more stable material for the fuel oxidation layer of OTMs.

Acknowledgements

The authors would like to thank Praxair for funding and Jonathan Lane for helpful discussions, we also acknowledge support from EPSRC for Platform Grant EP/K015540/1 and the Royal Society for Wolfson Merit Award WRMA 2012/R2.

The research data supporting this publication can be accessed at http://dx.doi.org/10.17630/e9ae1cc8-9e47-4caa-9d06-cc8a6adcd8d6.

References

[1] L. Rosen, et al., Energy Procedia 4 (2011) 750–755.
[2] D. Neagu, G. Tsekouras, D.N. Miller, H. Ménard, J.T.S. Irvine, Nat. Chem. 5 (2013) 916–923.
[3] T. Screen, Platin. Met. Rev. 51 (2007) 87–92.
[4] S. Tao, J.T.S. Irvine, S.M. Plint, J. Phys. Chem. 110 (2006) 21771–21776.
[5] T. Jardiel, et al., Solid State Ionics 181 (2010) 894–901.
[6] S. Boulfrad, M. Cassidy, E. Djurado, J.T.S. Irvine, G. Jabbour, Int. J. Hydrog. Energy 38 (2013) 9519–9524.
[7] N.K. Monteiro, F.B. Noronha, L.O.O. da Costa, M. Linardi, F.C. Fonseca, Int. J. Hydrog. Energy 37 (2012) 9816–9829.
[8] S. Tao, J.T.S. Irvine, Chem. Mater. 16 (2004) 4116–4121.
[9] Jen Hau Wan, J.H. Zhou, J.B. Goodenough, Electrochem. Soc. Proc. (2005) 429–434.
[10] S. Tao, J.T.S. Irvine, J. Electrochem. Soc. 151 (2004) A252.